scientific reports

Check for updates

OPEN

Effect of metal decoration on sulfur-based gas molecules adsorption on phosphorene

Yonghu Wang, Shuangying Lei✉, Ran Gao, Xiaolong Sun & Jie Chen✉

Based on first-principles calculation, the adsorption of sulfur-based gas molecules (H_2S, SO_2, SO_3) on various metal-decorated phosphorenes is researched systematically. Eleven metals (Li, Na, K, Rb, Cs, Ca, Sr, Ba, Ni, La, Tl) which can avoid the formation of clusters on the phosphorene are considered. Noticeably, all metal decorations can enhance the adsorption strength of phosphorene to sulfur-based gas molecules except for H_2S on Tl-decorated phosphorene. Meanwhile, the adsorption energy (E_{ads}) shows the trend of $E_{ads}(H_2S) < E_{ads}(SO_2) < E_{ads}(SO_3)$ for the same metal decoration case. In addition, some metal-decorated phosphorene systems exhibit intriguing magnetic and electrical variation after sulfur-based gas molecule adsorptions, indicating that these systems are promising to be candidates for the detection and removal of sulfur-based gas molecules.

Air pollution is becoming more and more serious with the rapid development of industrialization. Thanks to attenuation of organic substances, emission of sewage plants and burning of fossil fuels[1–4], every year more than billion tons of sulfur-based gases are discharged into the atmosphere[5,6]. The sulfur-containing gas compounds are all dangers for human-health[7–9]. SO_2 hurts the nerves in the respiratory system, including lesions in nasal cavity and throat. H_2S inhibits the metabolism of cells in the livers[10,11]. In terms of environmental pollution, sulfur-containing gas compounds can bring about sulfuric acid mist, sulphate aerosol, as well as acidic soil, which further harm animals and green plants[12,13]. Therefore, the treatment of sulfur-based exhaust gases is essential in environmental safety.

Adsorption is great competitive in the removal and detection of sulfur-based gases. A lot of experimental and theoretical investigations on the adsorption of sulfur-based gas compounds on metal and metal oxide are performed[14–16]. However, owing to the strict operating condition and low sensitivity, the metal and metal oxide are not the ideal candidate materials for sensing the sulfur-based gas compounds[17]. On the other hand, since the discovery of graphene in 2004[18–20], two-dimensional (2D) materials have aroused great interest of researchers owing to their superior mechanical, thermal, optical and electronic properties[21–24]. Another striking feature of 2D materials is the large surface-to-volume ratio, which may be attractive for gas detection and adsorption. Recently, the researchers observed that phosphorene has an advantage over graphene on the adsorption of small molecule gases because of its puckered surface morphology and higher surface-to-volume ratio[25,26]. Both theoretical and experimental researches have proven excellent gas sensing sensitivity of phosphorene[27,28]. However, the E_{ads} values of gases on pristine phosphorenes are too small, hence the surface decoration or/and doping is demanded to enhance the adsorption of gases[29–31]. For sulfur-based gas adsorption on phosphorene, the adsorptions of defective and metal substitute doped phosphorenes to H_2S and SO_2 were investigated by Kaewmaraya, which exposed that metal-dopings could significantly enhance the adsorption of phosphorene to SO_2[32].

In this investigation, we have systematically studied the adsorption of sulfur-based gas molecules (H_2S, SO_2, SO_3) on various metal-decorated phosphorene by using the first-principles calculation. To avoid clustering of metals on the surface of phosphorene, eleven metals have been opted on the basis of their bulk cohesive energy less than the binding energy. They are alkali (Li, Na, K, Rb, Cs), alkaline earth (Cs, Ca, Sr), transition (Ni, La), and post-transition (Tl) metals. Except for H_2S on Tl-decorated phosphorene, all metal decorations can improve the adsorption of sulfur-based gas molecules on phosphorene, especially Ni and Tl-decorated phosphorene. In addition, some metal-decorated phosphorene systems exhibit interesting magnetism and electrical transitions after SO_2 and SO_3 gas adsorption, which could have potential application for SO_2 and SO_3 gas detection.

Key Laboratory of Microelectromechanical Systems of the Ministry of Education, Southeast University, Nanjing 210096, China. ✉email: lsy@seu.edu.cn; seuc@seu.edu.cn

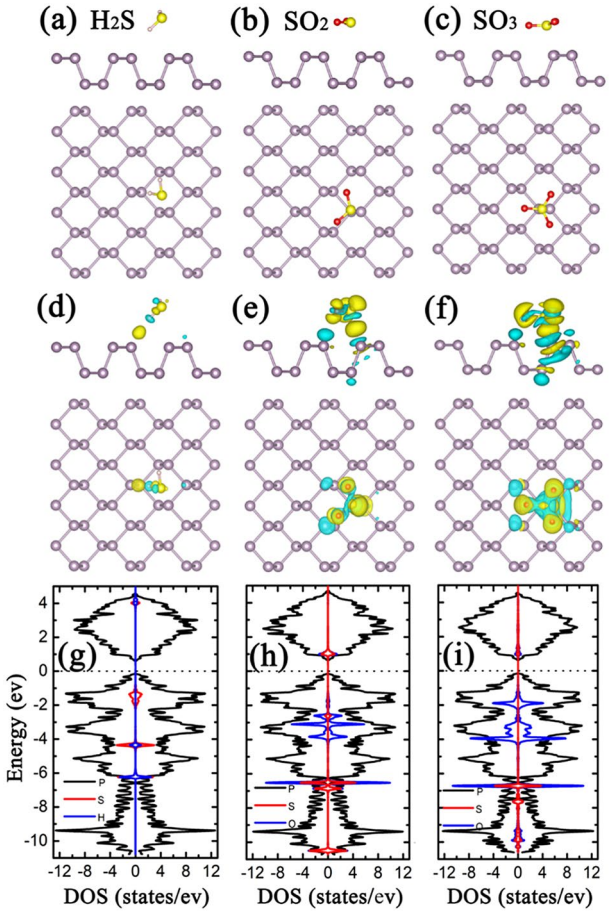

Figure 1. The optimized structure of (**a**) H_2S, (**b**) SO_2 and (**c**) SO_3 adsorbed 3×4 pristine phosphorene, (**d**–**f**) the DCD corresponding to (**a**–**c**), respectively, (**g**–**i**) the LDOS corresponding to (**a**–**c**), respectively. Purple, yellow, pink, and red balls in (**a**–**f**) represent P, S, H and O atoms, respectively. Yellow and blue regions in (**d**–**f**) denote charge accumulation and charge depletion, respectively. The black, red and blue curves in (**g**–**i**) represent LDOS of P, S and H (O), respectively, with the Fermi level set to zero.

Computational methods

In this article, all the density functional theory (DFT) calculations have been carried out by the Vienna ab initio simulation software package code (VASP)[33,34]. We took advantage of the Perdew-Burke-Ernzerhof (PBE) functional of generalized gradient approximation (GGA) to describe exchange–correlation interaction[35]. The van der Waals (vdW) interactions were dealt with by adopting empirical correction scheme of Grimme (DFT + D3)[36]. In all the calculations, the kinetic energy cut-off for the plane-wave basis was 500 eV. The 3×4 supercells and the vacuum distances of 15 Å were utilized to reduce the interaction of mirror adsorbates and phosphorene layers, respectively, and the corresponding k-point grids were set as $3\times3\times1$ by Monkhorst–Pack k-point scheme. The energy convergence accuracy was set to 10^{-5} eV, and all the structures were fully relaxed until the forces acting upon each atom were less than 0.01 eV/Å. For sulfur-based gas molecules adsorption on pristine phosphorene or metal-decorated phosphorene, the E_{ads} is calculated by the formula,

$$E_{ads} = E_{tot} - \left(E_{sub} + E_{gas}\right), \tag{1}$$

where E_{tot}, E_{sub} and E_{gas} are the energies of the adsorption system, substrate (pristine phosphorene or metal decorated phosphorene) and sulfur-based gas molecule (H_2S, SO_2, or SO_3), respectively.

Results and discussion

Sulfur-based gas molecules adsorption on pristine phosphorene. The lattice constants of the pristine phosphorene monolayer along the armchair and zigzag directions are 4.57 and 3.31 Å, respectively, with a direct bandgap of 0.88 eV, in agreement with previous studies[37,38]. For the adsorption of sulfur-based gas molecules (H_2S, SO_2, SO_3) on pristine phosphorene, various possible initial adsorption sites [e.g. hollow (H), bridge (B), top (T)] and adsorption configurations were considered [Figures S1–S3]. By comparing the total energies of the adsorption configurations after structural optimization, the configurations with the highest E_{ads} were obtained as shown in Fig. 1. The H_2S prefers to adsorb at the hollow site with H atoms pointing to the phosphorene surface, while the SO_2 and SO_3 prefer to adsorb at the T site lying parallel to the phosphorene surface.

Metal	E_{ads} (eV)			ΔQ (e)			$D_{sub\text{-}gas}$ (Å)		
	H_2S	SO_2	SO_3	H_2S	SO_2	SO_3	H_2S	SO_2	SO_3
bP	0.220	0.396	0.646	− 0.003	− 0.182	− 0.451	2.818	2.984	2.572
Li	0.695	1.213	1.684	− 0.080	− 0.626	− 1.004	2.484	2.003	1.952
Na	0.441	1.121	1.208	− 0.011	− 0.523	− 0.806	2.875	2.374	2.286
K	0.287	0.945	0.979	0.026	− 0.422	− 0.674	3.399	2.799	2.673
Rb	0.251	0.949	0.716	0.022	− 0.449	− 0.526	3.610	2.978	2.640
Cs	0.208	0.810	0.828	0.019	− 0.399	− 0.640	3.844	3.182	3.001
Ca	0.584	2.086	3.657	0.014	− 0.862	− 1.416	2.963	2.263	2.147
Sr	0.485	1.929	3.419	0.010	− 0.830	− 1.435	3.193	2.439	2.295
Ba	0.686	1.657	3.232	− 0.059	− 0.801	− 1.484	3.307	2.633	2.591
Ni	1.158	1.304	1.605	0.042	− 0.318	− 0.724	2.207	2.074	1.977
La	0.773	2.822	4.508	− 0.044	− 1.157	− 1.325	3.136	2.272	2.175
Tl	0.136	0.597	1.273	0.021	− 0.418	− 0.832	3.795	2.978	2.721

Table 1. The E_{ads} values of sulfur-based gas on phosphorene and bP-Ms. The ΔQ and $D_{sub\text{-}gas}$ between sulfur-based gas and substrates.

Such a phenomenon may be attributed to the larger electronegativity of O compared with H. The nearest atom-to-atom distances between H_2S, SO_2 and SO_3 and the surface of the phosphorene are 2.818, 2.984 and 2.572 Å, respectively. The E_{ads} values of H_2S, SO_2 and SO_3 on phosphorene, calculated using Eq. (1), are 0.220, 0.396 and 0.646 eV, respectively. To analyze the mechanism of interaction between sulfur-based gas molecules and phosphorene, the differential charge density (DCD) of the most stable adsorption configurations were calculated, as illustrated in Fig. 1d–f. It can be seen that, from H_2S to SO_2 to SO_3, the electron accumulations around gas molecules increase significantly, which are also confirmed by the Bader charge analysis. The Bader charge analysis shows that the electrons transferred from the phosphorene to H_2S, SO_2 and SO_3 molecules are 0.003, 0.182 and 0.451 e, respectively, ascribing to higher electronegativity of gas molecules over the phosphorene. Generally, the more charge quantities transferred means the stronger interactions, and thus the larger E_{ads} values[39]. Here, the variation trend of charge quantities transferred does agree with that of the E_{ads} values (see Table 1).

To understand the effect of the adsorption of sulfur-based gas molecules on the electrical properties of phosphorene, the local density of states (LDOS) of the adsorption system were calculated, as shown in Fig. 1. In LDOSs, the DOS near the Fermi level is zero for all three adsorption systems, indicating the adsorption of sulfur-based gas don't change the phosphorene's electronic structure. The bandgaps of phosphorenes are 0.86 and 0.87 eV, respectively, after H_2S and SO_2 adsorptions, which are marginally smaller than that of pristine one, while the bandgap of phosphorene slightly increase to 0.89 eV after SO_3 adsorption. After sulfur-based gas molecule adsorptions, the slight variation of bandgap may be ascribed to the change of channel of phosphorene. It has been pointed out that a narrower channel (3.49 Å for H_2S and 3.44 Å for SO_2 as compared to 3.54 Å for pristine phosphorene) would result in the stronger repulsive interaction between the facing lone pairs at the ditch of phosphorene and thus the decrease of bandgap, and vice-versa[40]. For H_2S adsorption case, the H atom is the nearest to the P atom, but the H atomic DOS is far from the Fermi level, which should be also responsible for the smaller E_{ads} value. In the case of SO_2 and SO_3, the S atoms are the closest to P atoms. Near Fermi levels, the S DOS peak is just above the conduction band minimum. Especially for SO_3, the S DOS distributes widely in the conduction band, which should be responsible for the largest E_{ads} values among the three adsorption cases. The adsorption energy closed to 1 eV is an ideal binding for the efficient and reversible gas sensor. However, the E_{ads} values of sulfur-based gas molecules on pristine phosphorene are too small for this purpose. The metal decoration can improve the adsorption of gas, so we will discuss the metal decorations and the sulfur-based gas molecule adsorptions on metal decorated phosphorenes.

Sulfur-based gas molecules adsorption on bP-Ms. The theoretical studies have shown that metal decoration can significantly influence the electronic properties of phosphorene[41]. It is well-known if the E_{ads} value of a metal on 2D materials is less than its bulk cohesive energy (E_{coh}), it is going to cluster on the 2D surfaces. Therefore, to enhance the adsorption of sulfur-based gas on phosphorenes and avert clustering of metal atoms on the surface, eleven metals (Li, Na, K, Rb, Cs, Ca, Sr, Ba, Ni, La, Tl) have been opted to decorate the phosphorene on the basis of $E_{ads}/E_{coh} > 1$[42]. Here, the electronic properties of black phosphorenes decorated with metals (bP-Ms) are discussed first to contrast before and after sulfur-based gas molecule adsorptions. Figure 2 shows the band structures and projected density of states (PDOSs) of the bP-Ms. Except for Ni, the outermost *s*-states of alkali metals (AMs = Li, Na, K, Rb, Cs) and those of alkaline earth metals (AEMs = Ca, Sr, Ba), the 6 *p*-state of Tl and 5 *d*-state of La are mainly distributed in the conduction band of phosphorenes, which cause valence-electron transfer from metals to phosphorenes, and thus the Fermi levels shift up in energy. For AM decorated and Tl decorated phosphorenes (bP-AMs and bP-Tl), the Fermi levels shift upward into the conduction bands of phosphorenes and the corresponding bP-AMs and bP-Tl show metal properties. The *s*-states of AMs and *p*-state of Tl are far above the lowest conduction bands of phosphorenes. Unlike the AMs and Tl, the *s*-states of AEMs or *d*-state of La are aligned to the lowest conduction band of phosphorene, which causes a strongly repulsive interaction between metal atomic states and the lowest conduction bands of phosphorenes, so

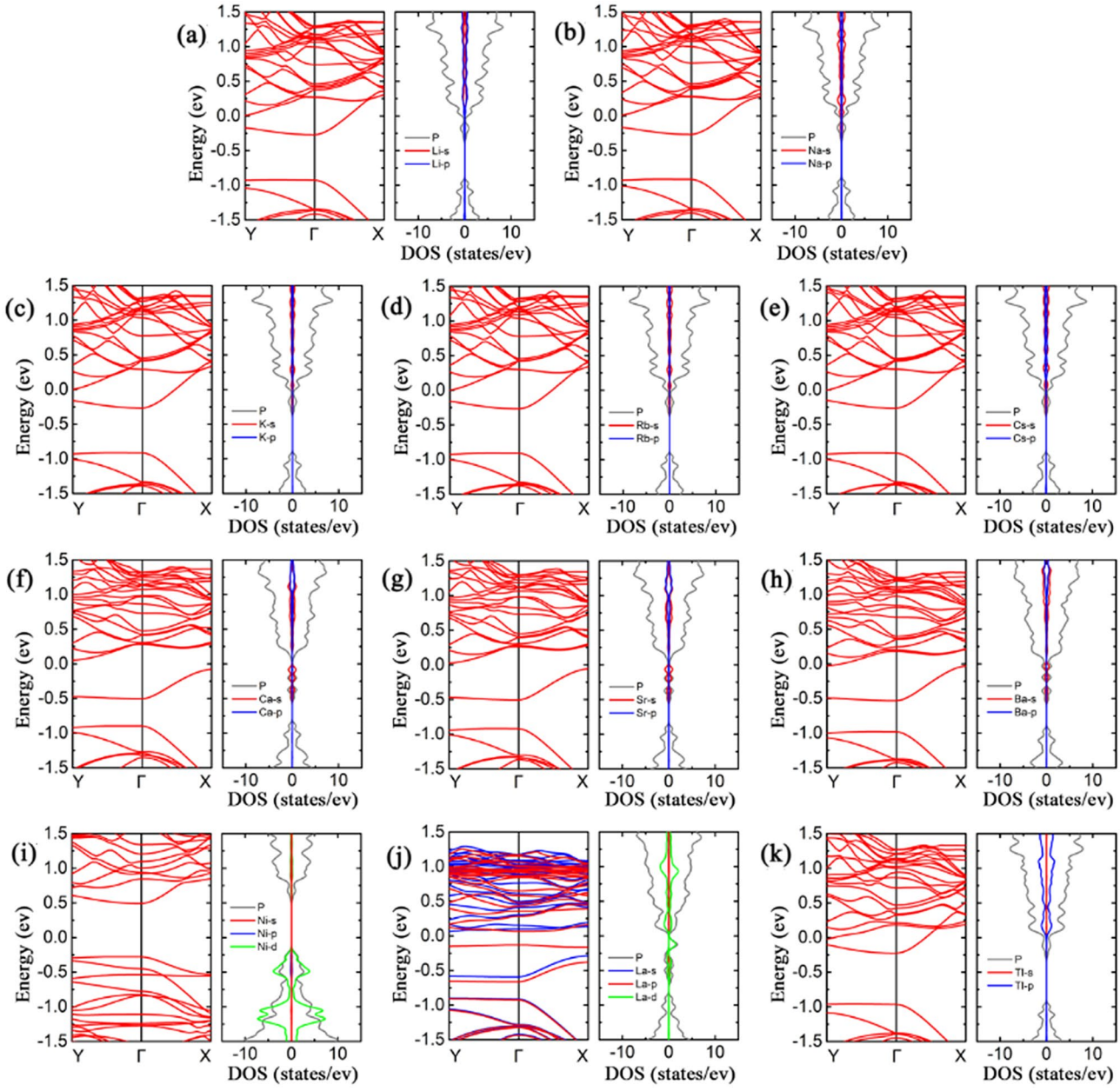

Figure 2. The band structures and projected DOSs of (**a**) bP-Li, (**b**) bP-Na, (**c**) bP-K, (**d**) bP-Rb, (**e**) bP-Cs, (**f**) bP-Ca, (**g**) bP-Sr, (**h**) bP-Ba, (**i**) bP-Ni, (**j**) bP-La and (**k**) bP-Tl. The red and blue curves represent the spin-up and spin-down bands, respectively. The gray curves in projected DOS represent state of P, and the red, blue and green curves represent the *s*-, *p*- and *d*-states for metal atoms.

the lowest conduction bands are pushed down. As a consequence, there are large separations between the lowest and second lowest conduction bands for AEM decorated phosphorenes (bP-AEMs) and bP-La. On the other hand, the more *s*- and *d*-electrons transfer for bP-AEMs and bP-La, the more energies shift for Fermi levels. The Fermi levels of bP-AEMs and bP-La are located between the lowest and second lowest conduction bands. The bP-Ca, bP-Sr and bP-La show semiconductor properties, while bP-Ba shows metal property due to that the Fermi level cross slightly through the second lowest conduction band of phosphorene. Additionally, bP-La has spin-polarized LDOS (Fig. 2), with magnetic moment of 1 μ_B. For Ni decorated case, the *s*- and *d*- states are distributed in valence band of phosphorene, and the semiconductor property of bP-Ni is remained. However, the bandgap of bP-Ni decreases to 0.769 eV as compared with that of pristine phosphorene, which may be ascribed to the strong hybridized interaction between Ni *d*-state and valence band of phosphorene, and thus the highest valence band is pushed upward.

H_2S gas molecules adsorption on bP-Ms. For the H_2S adsorption on bP-Ms (M = Li, Na, K, Rb, Cs, Ca, Sr, Ba, Ni, La, Tl), the various initial configurations are considered and are fully optimized. By comparing the E_{ads} values, the most stable structures, namely the structures with the largest absolute E_{ads} values, are achieved as

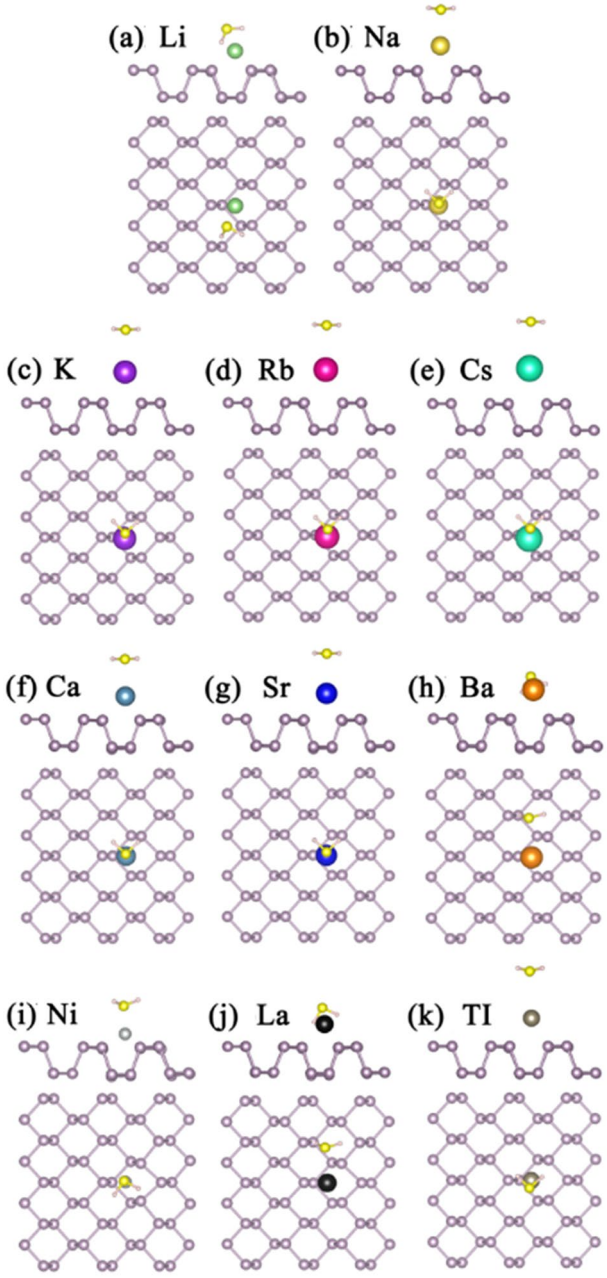

Figure 3. The optimized structures of H_2S adsorption on (**a**) bP-Li (**b**) bP-Na (**c**) bP-K (**d**) bP-Rb (**e**) bP-Cs (**f**) bP-Ca (**g**) bP-Sr (**h**) bP-Ba (**i**) bP-Ni (**j**) bP-La (k) bP-Tl. The green, gold, purple, red, cyan, dark cyan, blue, orange, light gray, black and gray balls represent Li, Na, K, Rb, Cs, Ca, Sr, Ba, Ni, La and Tl, respectively.

shown in Fig. 3. In all the structures, the distances between the sulfur and metal atoms are apparently nearer than those between H and metal atoms. Except for bP-Li, bP-Ba and bP-La systems, H_2S is adsorbed on the bP-Ms in parallel to the surface of phosphorene. The E_{ads} values of S-based gases, the charge transfer amounts (ΔQ) and adsorption distances ($D_{sub\text{-}gas}$) between sulfur-based gas molecules and substrates are summarized in Table 1. As compared with the adsorption energy of 0.220 eV for H_2S on pristine phosphorene, except for Cs and Tl atoms, the decorations of the rest metals enhance the adsorption of phosphorene to H_2S. Especially, the E_{ads} value of H_2S on bP-Ni is up to 1.158 eV (see Table 1), which is the largest value for all the H_2S adsorption systems. Correspondingly, the adsorption distance between Ni and S atoms is the smallest among the adsorption of H_2S on the metal decorated phosphorene, and the value is 2.207 Å. However, the adsorption energies of H_2S on bP-Tl and bP-Cs are the smallest, even smaller than that on pristine phosphorene. On the one hand, it may be due to the fact that the electrons of all atoms in H2S molecule are full shell structure, resulting in less charge transfer and interaction; On the other hand, it may be attributed to the relatively large atomic radii of Tl and Cs, which cause the longer adsorption distance as well as less interaction between gas and metal decorated phosphorene.

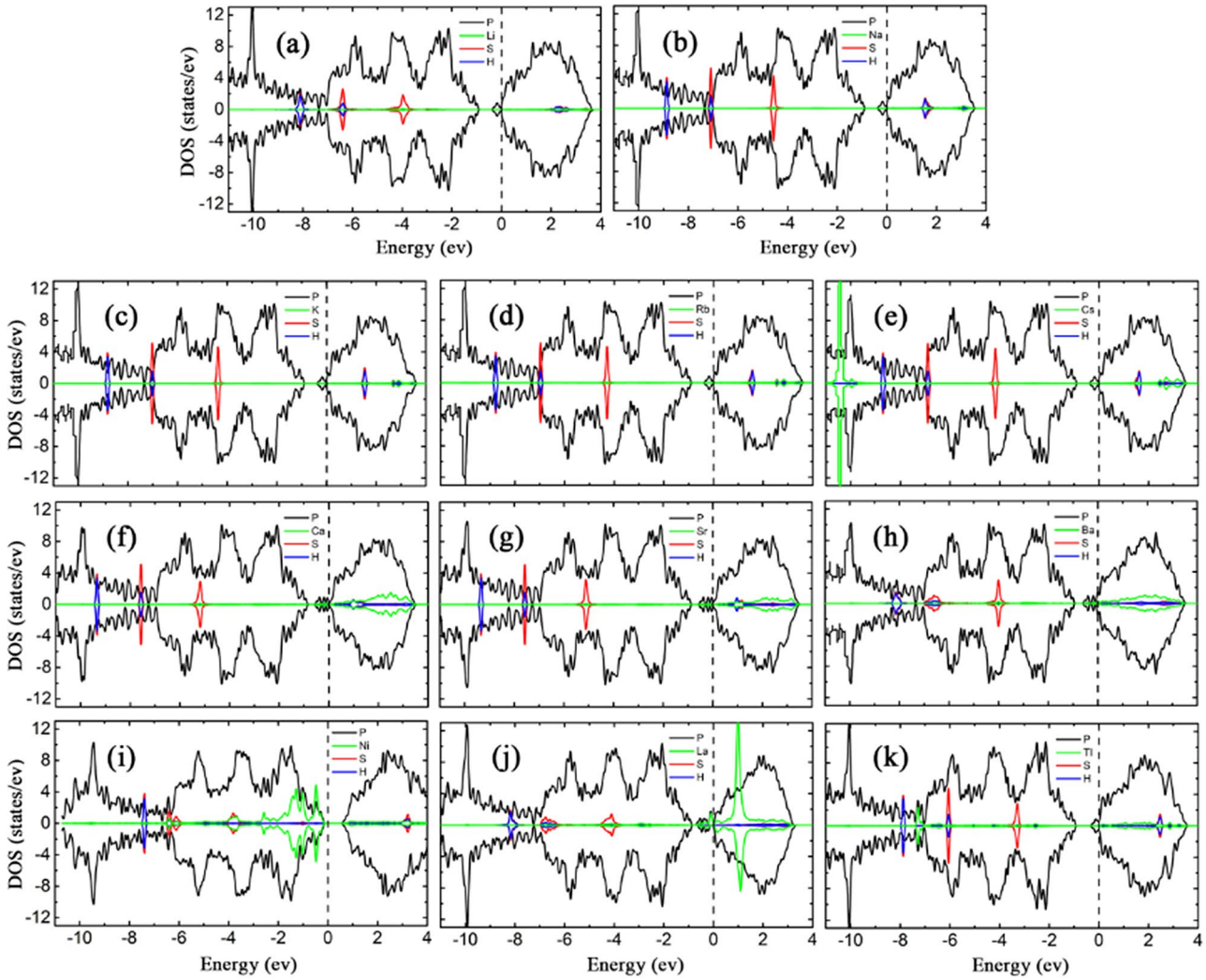

Figure 4. The LDOSs of H_2S adsorption on (**a**) bP-Li (**b**) bP-Na (**c**) bP-K (**d**) bP-Rb (**e**) bP-Cs (**f**) bP-Ca (**g**) bP-Sr (**h**) bP-Ba (**i**) bP-Ni (**j**) bP-La (k) bP-Tl. The black, green, red and blue curves represent LDOS of P, metal, S and H, respectively, with the Fermi level set to zero.

The H_2S on bP-Tl and bP-Cs have the largest adsorption distance of 3.795 and 3.844 Å, respectively, which may be due to the larger Tl atomic size.

To understand the mechanism of adsorption-energy enhancement and the effect of H_2S on the electronic and magnetic properties of bP-AM, the LDOSs of the adsorption systems were calculated, as shown in Fig. 4. The magnetic moment of bP-La reduces slightly from 1.00 to 0.98 μ_B after H_2S adsorption, while those of the other bP-Ms systems remain zero, which are corroborated by the spin asymmetric LDOS for H_2S adsorbed bP-La and the spin symmetric LDOSs for the other H_2S adsorbed bP-M systems. Except for Ca, Sr and La decorated cases, the adsorptions of H_2S have no effect on the electronic properties of the rest bP-M systems. The metal or semiconductor properties of the rest bP-M systems remained after H_2S adsorption. The adsorption of H_2S enhances the interaction between Ca/Sr atom and the conduction band of phosphorene, which leads to a slight downward shift of the conduction band and the Fermi energy level entering the sub-low conduction band, and further causes that bP-Ca and bP-Sr undergo the transformation from semiconductor to metal after the adsorption of H_2S molecule. As shown in Fig. 4, there are the overlapping peaks between the sulfur and metal atoms located near − 5 or − 4 eV for AMs, AEMs and La decorated cases, which should be a reason of the improved H_2S adsorption. The smallest E_{ads} values for Cs and Tl decorated may be mainly attributed to the large radii of Cs and Tl atoms. For Ni decorated case, the apparent overlapping peaks of S and Ni atoms near − 6, − 4 and − 1 eV imply the strong hybridized interaction between H_2S and bP-Ni substrate, which may be primarily responsible for the largest E_{ads} value. Additionally, the states of S and H atoms are far from the Fermi level, implying that H_2S adsorption almost has no effect on the band structures near it for bP-Ms. Thus, the conductivity properties of bP-Ms are not changed by H_2S adsorption except for Sr and La decorated cases. For Sr decorated case, the state of H_2S molecule in conduction band pushes slightly the conduction band minimum of bP-Sr down, which makes the small bandgap (0.07 eV) of bP-Sr disappear. For La decorated case, the charge transfer from substrate to H_2S makes the Fermi level shift down in energy after H_2S adsorption, and finally the Fermi level

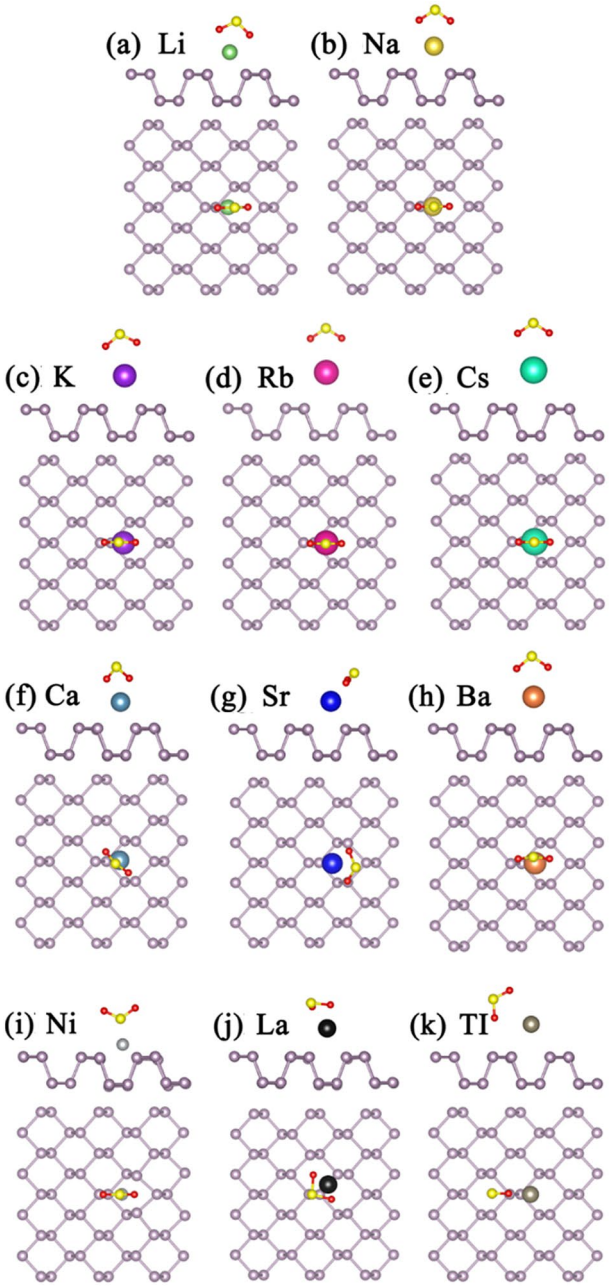

Figure 5. The optimized structures of SO_2 adsorption on (**a**) bP-Li (**b**) bP-Na (**c**) bP-K (**d**) bP-Rb (**e**) bP-Cs (**f**) bP-Ca (**g**) bP-Sr (**h**) bP-Ba (**i**) bP-Ni (**j**) bP-La (k) bP-Tl. The green, gold, purple, red, cyan, dark cyan, bule, orange, light gray, black and gray balls represent Li, Na, K, Rb, Cs, Ca, Sr, Ba, Ni, La and Tl, respectively.

crosses through the spin-up band [see the red curve below the Fermi level in Fig. 2(j)], which leads to the half-metal property of bP-La.

SO_2 gas molecules adsorption on bP-Ms. For the SO_2 adsorption on bP-Ms, the most stable structures are illustrated in Fig. 5. Except for SO_2 adsorption on bP-Ni, the SO_2 preferably adsorbs on the bP-AMs with bond angles toward the metal atoms, and oxygens of SO_2 are the nearest atoms to the metal atoms. As given in Table 1, all the metal decorations can significantly improve the adsorption capacity of phosphorene to SO_2. The corresponding E_{ads} values vary from 0.597 to 2.822 eV, and stay larger than the pristine phosphorene case of 0.396 eV. In addition, we can see that the decoration of AEMs (Ca, Sr, Ba) is more effective than AMs (Li, Na, K, Rb, Cs) for adsorbing SO_2 due to larger E_{ads} values (Table 1), and that decrease with atomic number in the same group elements. As we know, the more charge transfer means the stronger interaction, i.e. larger E_{ads} value. Consequently, the more valence electrons of AEMs and thus the more electron transfers should be in charge of their larger E_{ads} values. On the other hand, short adsorption distance is beneficial for the charge transfer. Thus,

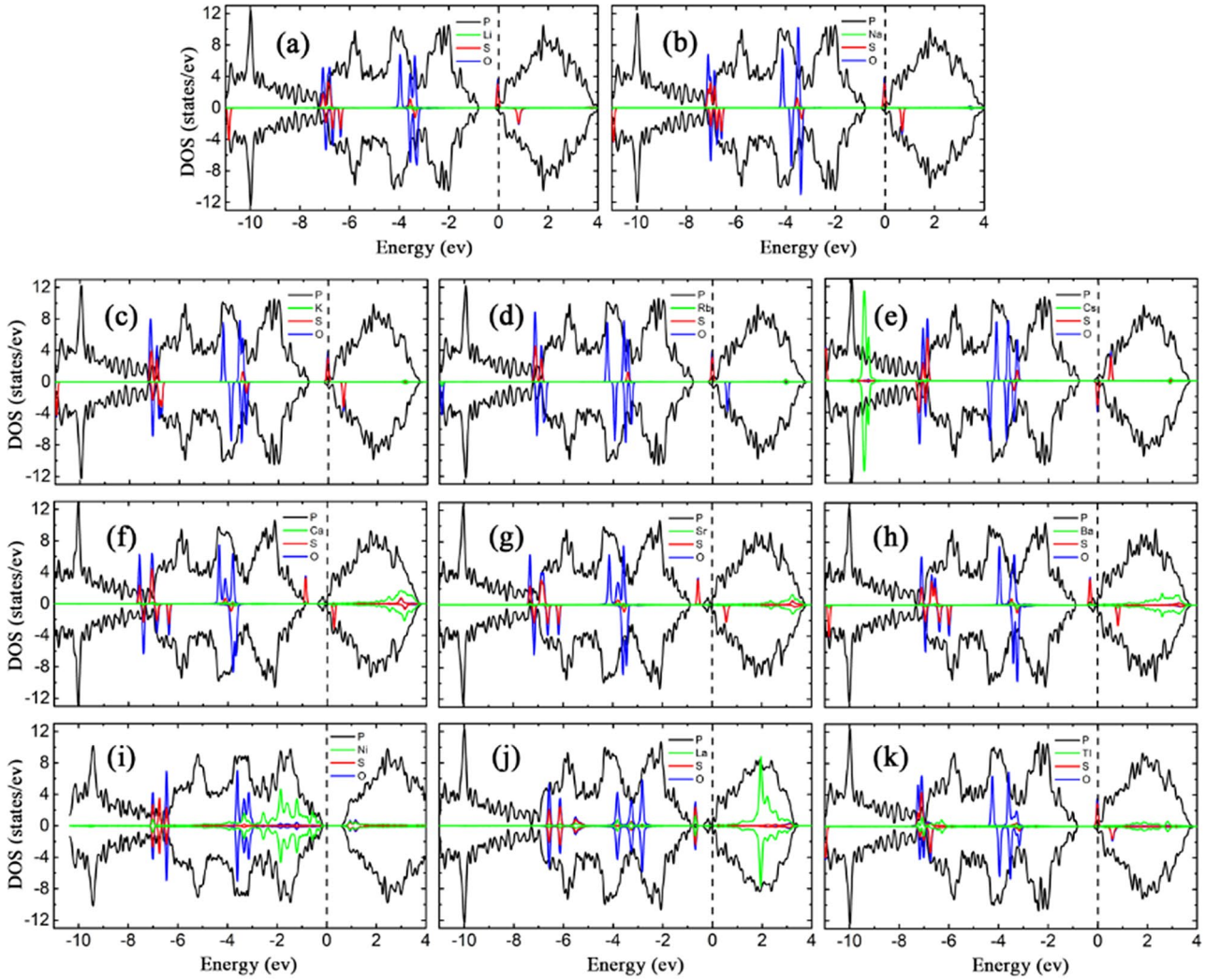

Figure 6. The LDOSs of SO_2 adsorption on (**a**) bP-Li (**b**) bP-Na (**c**) bP-K (**d**) bP-Rb (**e**) bP-Cs (**f**) bP-Ca (**g**) bP-Sr (**h**) bP-Ba (**i**) bP-Ni (**j**) bP-La (k) bP-Tl. The black, green, red and blue curves represent the LDOS of P, metal, S and O, respectively, with the Fermi level set to zero.

an increasing adsorption distance should be responsible for decreasing E_{ads} values in the same group elements. Adsorption distance may be attributed to the atomic radius increasing with atomic number.

To understand how the SO_2 effect on the properties of the metal decorated substrates, the LDOSs of all SO_2 adsorption systems were calculated and shown in Fig. 6. The non-zero LDOSs at the Fermi level imply the metal properties for SO_2 adsorptions on bP-AM, bP-AEM, bP-La and bP-Tl systems, while the zero LDOSs at the Fermi level imply semiconductor properties for that on bP-Ni system. Except for bP-Ni, almost all the bP-Ms exhibit spin asymmetry after SO_2 adsorption. The SO_2 adsorbed bP-La has a negligible magnetic moment of 0.0002 μ_B, on the spin polarization of bP-La system is suppressed by the SO_2 adsorption. Thus, the bP-AMs, bP-AEMs and bP-Tl perceive magnetization on SO_2 adsorption, while bP-La loses the magnetization. In addition, the bP-Ca, bP-Sr and bP-La become metallic, on upward movement of the lowest conduction band of phosphorene (see figure S6 in supporting materials). In fact, upward movements of the lowest conduction bands exist in all the SO_2 adsorbed bP-M systems, including the SO_2 adsorption on bP-AM, bP-Ba and bP-Tl systems (although their metal properties remained), which may be attributed to that the SO_2 adsorptions weaken the interactions between the metals and phosphorenes. For SO_2 adsorption on bP-Ni, upward movement of the lowest conduction band results in that the bandgap of bP-Ni rises from 0.769 to 0.876 eV after SO_2 adsorption. On the other hand, as compared with before SO_2 adsorption, the electron transfers from bP-M systems to SO_2 lead to downward shifts of the Fermi levels for bP-M systems, which may be ascribed to the greater electronegativity of S and O atoms. Except for Ni decorated case, the peaks of O states appear near the Fermi levels, which will introduce the flat bands into the band structures for SO_2 adsorption on bP-Ms (see figure S6). As compared with SO_2 adsorption on the AM systems, the coupling peaks between SO_2 and AEMs are more widely distributed, especially in the conduction band (Fig. 6), which may be a reason of more effectively improving SO_2 adsorption on phosphorene for the AEM decorated cases. Strong hybridized interaction between the states of SO_2 and La at − 0.8 eV in Fig. 6j can unravel a maximal E_{ads} = 2.822 eV for SO_2 adsorption on bP-La.

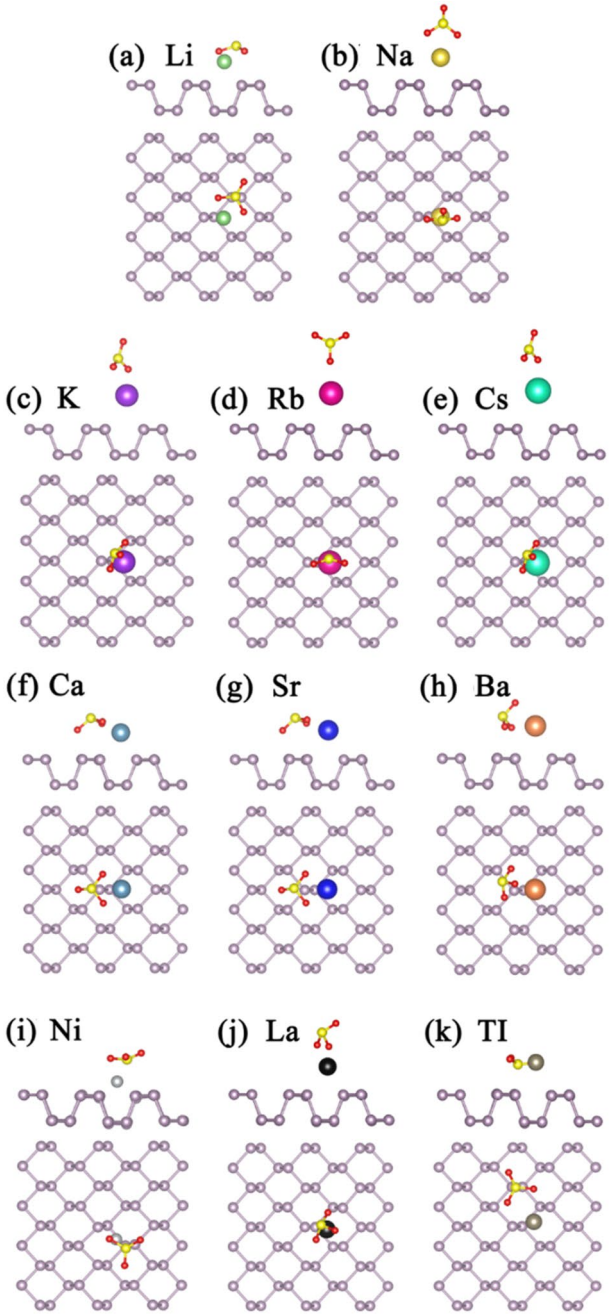

Figure 7. The optimized structures of SO_3 adsorption on (**a**) bP-Li (**b**) bP-Na (**c**) bP-K (**d**) bP-Rb (**e**) bP-Cs (**f**) bP-Ca (**g**) bP-Sr (**h**) bP-Ba (**i**) bP-Ni (**j**) bP-La (k) bP-Tl. The green, gold, purple, red, cyan, dark cyan, bule, orange, light gray, black and gray balls represent Li, Na, K, Rb, Cs, Ca, Sr, Ba, Ni, La and Tl , respectively.

SO_3 gas molecules adsorption on bP-Ms. Optimized structures of SO_3 adsorption on bP-Ms in different initial configurations are shown in Fig. 7. Compared to H_2S and SO_2, the most stable adsorption configurations of SO_3 on bP-Ms are more diverse and have larger E_{ads} values for the same metal decorated substrate. However, in all the adsorption configurations of SO_3 on bP-Ms, the O in SO_3 is the nearest to metal atoms. The corresponding adsorption energies of 0.716 to 4.508 eV (Table 1) are larger than the 0.646 eV value of SO_3 on pristine phosphorene. Especially, the adsorption configuration of SO_3 on bP-Tl is similar to that on pristine phosphorene, but the E_{ads} value increases from above value of pristine phosphorene to 1.273 eV due to the Tl atomic decoration. Thus, all the metal decorations significantly improve the SO_3 adsorption on phosphorene. Similar to SO_2, E_{ads} values of SO_3 on bP-AEM are larger than that on bP-AM, indicating more efficient decorations of AEMs than AMs in improving the SO_3 adsorption on phosphorene. As mentioned above, the more charge transfer signifies the stronger interaction and in turn the larger E_{ads} value[39]. Consequently, the more valence electrons of AEMs and thus electron transfers should be responsible for their larger E_{ads} values. On the other hand, in the same

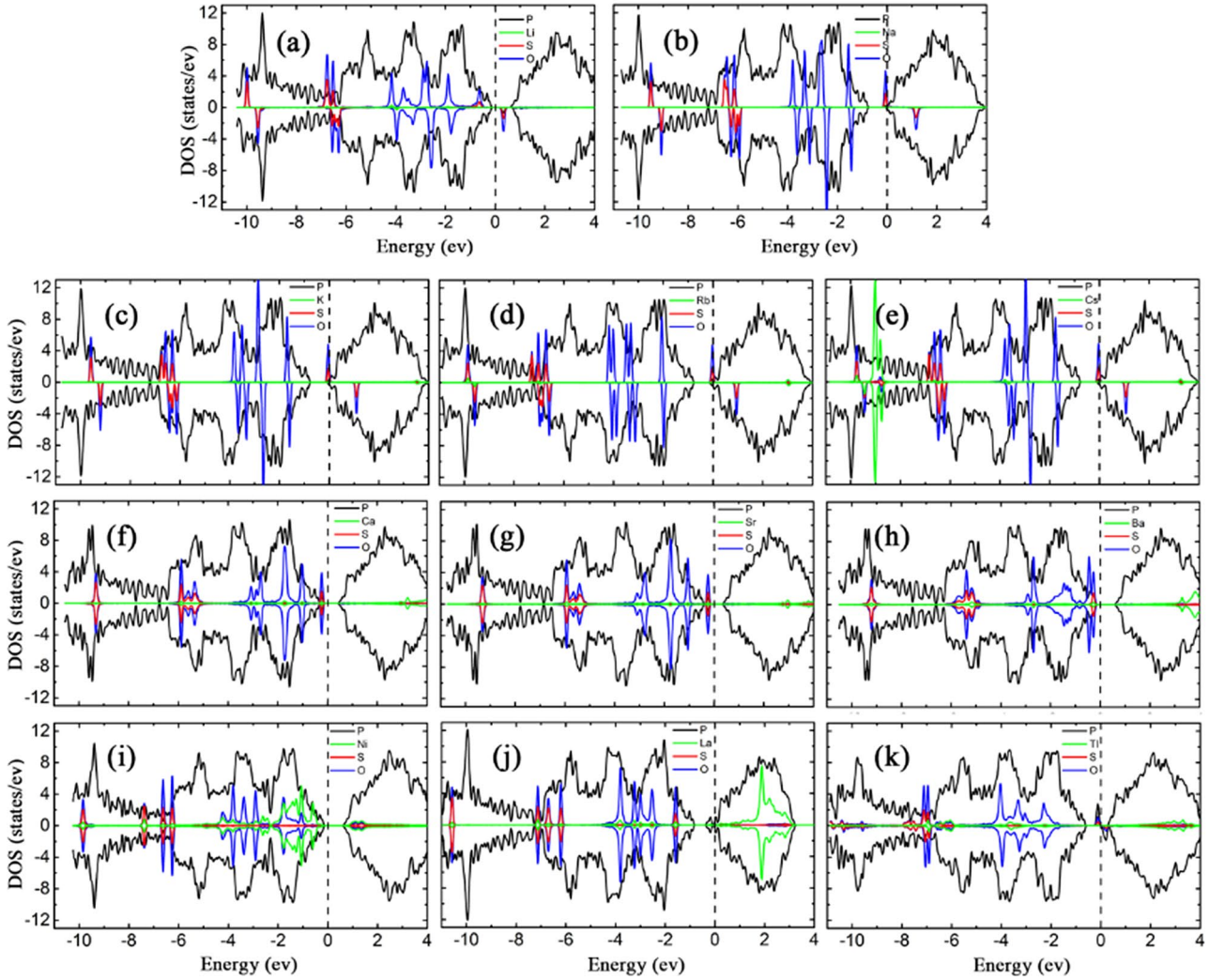

Figure 8. The LDOSs of SO_3 adsorption on (**a**) bP-Li (**b**) bP-Na (**c**) bP-K (**d**) bP-Rb (**e**) bP-Cs (**f**) bP-Ca (**g**) bP-Sr (**h**) bP-Ba (**i**) bP-Ni (**j**) bP-La (k) bP-Tl. The black, green, red and blue curves represent the LDOS of P, metal, S and O, respectively, with the Fermi level set to zero.

group elements, the E_{ads} values decrease with the atomic number in lieu of increasing atomic size. As mentioned before, short adsorption distance is advantageous to the charge transfer[26,27]. The larger atomic size means the larger adsorption distance and thus the more charge transfer, leading to larger interaction and larger E_{ads} value. Additionally, we can see (Table 1) the electrons transfer from bP-Ms to SO_3 in SO_3 adsorbed bP-Ms, in accords to larger S and O electronegativities.

In Fig. 8, LDOSs of SO_3 adsorbed bP-Ms display marked effects of SO_3 on the bP-Ms substrates. The LDOSs of bP-AMs and bP-Tl reveal significant spin asymmetry after SO_3 adsorptions, which are duly induced by SO_3, indicating magnetism in the SO_3 adsorbed bP-AMs and bP-Tl. The SO_3 adsorbed bP-AEMs and bP-Ni have spin symmetrical LDOSs and no magnetism. The magnetic moment of SO_3 adsorbed bP-La is only 0.0003 μ_B, which can be ignored with almost spin symmetrical LDOSs. Therefore, the bP-AMs and bP-Tl develop magnetism on SO_3 adsorption, while the bP-La adversely loses the magnetism. The SO_3 adsorbed bP-Li, bP-Na, bP-AEMs, bP-Ni and bP-Tl systems have zero DOSs at the Fermi levels of semiconductor properties. The SO_3 adsorbed bP-K, bP-Rb, bP-Cs and bP-La have non-zero DOSs at the Fermi levels, implying that they possess metal properties. In contrast to before SO_3 adsorption, the bP-Li, bP-Na, bP-Ba and bP-Tl develop metal-to-semiconductor transitions after SO_3 adsorption, while the bP-La develops the semiconductor-to-metal transition. As showed in figure S7 of supporting materials, the effect of SO_3 on the band structures of bP-M systems is the largest among the three gas molecules, likely due to the largest amount of electron transfer from the bP-Ms substrate to SO_3.

In addition, the SO_3 introduces impurity states into/near bandgaps or into the valence bands. Accordingly, the Fermi levels of bP-Ms shift down differently as a result of a charge transfer from the substrate to SO_3. As shown in Fig. 8a,b, the highest spin-up states of SO_3 for bP-Li and bP-Na systems are located in valence and bandgap, respectively, and both are below the Fermi levels. This leads to more electron transfer from bP-Li and bP-Na to SO_3, a way in witch bP-Li and bP-Na have restored to be semiconductor, which is responsible for their metal-to-semiconductor transitions. But for bP-K, bP-Rb and bP-Cs systems, as shown in Fig. 8c–e, the highest spin-up SO_3 states cross through the lowest conduction bands of bP-Ms, leading to less electrons transfer and

Metal	bP-M			H_2S-bP-M			SO_2-bP-M			SO_3-bP-M		
	M	E_g	D/I	*M*	E_g	D/I	*M*	E_g	D/I	*M*	E_g	D/I
Li	0	0		0	0		0.71	0		1.00	0.896/0.493	D/I
Na	0	0		0	0		0.58	0		0.92	0.094/0.839	I
K	0	0		0	0		0.50	0		0.81	0	
Rb	0	0		0	0		0.50	0		0.61	0	
Cs	0	0		0	0		− 0.46	0		0.76	0	
Ca	0	0.119	I	0	0.05	I	0.99	0		0	0.710	I
Sr	0	0.071	I	0	0		0.99	0		0	0.626	I
Ba	0	0		0	0		1.00	0		0	0.868	D
Ni	0	0.769	D	0	0.858	D	0	0.876	D	0	0.882	I
La	1.00	0.116/0.299	I	0.98	0/0.210	I	0	0		0	0	
Tl	0			0			0.51			0.99	0.417/0.738	I

Table 2. The magnetic moment (*M*), bandgap (E_g), and direct/indirect bandgap (D/I) of sulfur-based gas on phosphorene and bP-Ms. The units of *M* and E_g are μ_B and eV, respectively.

thus metal properties being remained. For bP-AEM, both the highest spin-up and spin-down bands are located near valence band maximum (VBM) and below the Fermi levels, resulting in that the Fermi levels shift down due to electrons transferring from bP-AEM to SO_3. On the other hand, the AEM – SO_3 interaction weakens the corresponding AEM – phosphorene interactions, and thus the lowest conduction band moves upward and the energy separation between the lowest and the second lowest conduction bands restores to pristine phosphorene value. Consequently, the bP-AEMs show semiconductor properties after SO_3 adsorption, and complete the metal-to-semiconductor transitions. For SO_3 adsorbed bP-Ni system, the bandgap of bP-Ni system increases to 0.882 eV due to the AEM – SO_3 interaction. The VBM is transferred from Γ point to Y point, and thus the bP-Ni exhibits indirect semiconductor properties and experiences a direct-to-indirect transition. For SO_3 adsorbed bP-La system, the metal flat band disappears and thus the lowest conduction band shifts upward owing to the La – SO_3 interaction on phosphorene. This leads to the metal → semiconductor transition of the bP-Tl system after SO_3 adsorption. This may be ascribed to the SO_3 flat bands in bandgap of bP-Tl, which push upward the lowest conduction band. Compared to the LDOS of SO_3 adsorbed bP-AM systems, the coupling peaks between SO_3 – metals are more widely distributed at − 9 eV, − 6 to − 5 eV, − 3 to 0 eV and in the conduction band, which also may be a reason of AEM decoration is more effective in improving the SO_3 adsorption on phosphorene. For SO_3 adsorbed bP-Ni, bP-La and bP-Tl systems, there are many coupling peaks between the states of metal and SO_3 near the Fermi level, which may be responsible for the large interactions between bP-Ms and SO_3. As compared with other metal cases, more coupling peaks of La and SO_3 are located in the band, contributing to the excellent SO_3 adsorption performance on the bP-La surfaces.

The values of magnetization and bandgap obtained in the various samples with H_2S, SO_2 and SO_3 adsorption on phosphorene of various metal decorations are summarized in Table 2. As mentioned above, a larger E_{ads} value above 1.5 eV is suitable for capturing gas molecules (or single sensing), whereas that near around 1 eV is ideal binding for highly efficient and reversible gas sensors. Therefore, from Table 1, one can see that the phosphorenes with AEM and La decorations can be served as capturing the SO_2 and SO_3 molecules, and that those with Li and Ni decorations can only be utilized as the SO_3 capture. From Table 2, it is observed that the Li, Ca, Sr and Ba decorated phosphorenes can be used as selective single sensing for SO_3 on the basis of increase of bandgap and thus decrease of conductivity after SO_3 adsorption.

The E_{ads} values of H_2S on K, Rb, Cs and Tl decorated phosphorenes are so small that H_2S gases are easy to dissociate from substrates, and thus the K, Rb, Cs and Tl decorated phosphorenes are not suitable for H_2S sensing. In addition to the moderate E_{ads} value, the change in measurable property is necessary for reversible gas sensors. Therefore, the Tl decorated phosphorene is promising to be a selective reversible SO_3 sensor due to the metal-to-semiconductor transition after gas molecule adsorption, while the semiconductor-to-half-metal transition of the La decorated phosphorene makes it be the potential candidate as a selective reversible H_2S sensor. Interestingly, it is found that the magnetic moment turns positive and negative, respectively, after SO_2 and SO_3 adsorptions, which may be a basis of selectively sensing these gases.

Conclusions

In summary, the adsorption of H_2S, SO_2 and SO_3 on various metal-decorated phosphorene have been systematically investigated by using DFT. Eleven metals (Li, Na, K, Rb, Cs, Ca, Sr, Ba, Ni, La, Tl), $E_{ads}/E_{coh} > 1$, are considered. Excepting H_2S on bP-Tl, a decoration of metals has significantly improved the adsorption of phosphorene to sulfur-based gas molecules, and the order of adsorption capacity is La > AEM > AM. In the analysis of LDOSs, it is found that the phosphorenes with Sr and La decorations undergo the transitions from semiconductor to metal and from semiconductor to half-metal after H_2S adsorption. The AM, AEM and Tl decorated phosphorenes undergo non-magnetic-to-magnetic transitions, after SO_2 adsorption, while the La decorated phosphorene undergoes magnetic-to-non-magnetic transition. Meantime, the Ca, Sr and La decorated phosphorenes also have transition from semiconductor to metal after SO_2 adsorption. For SO_3 adsorption cases, the AM and Tl decorated phosphorenes obtain non-magnetic-to-magnetic transitions, while the La decorated phosphorene perceive the

transition from magnetic to non-magnetic. The Li, Na and AEM decorated phosphorenes experience the transitions from metal to semiconductor, while the La decorated phosphorene experiences semiconductor-to-metal transition. On the basis of the criterion of adsorption energy around 1 eV and the changes in properties, the phosphorenes with La and Tl decorations are promising selective reversible sensors for H_2S and SO_3 detections, respectively. According to whether the magnetic moment is positive or negative, the Cs decorated phosphorene could be a potential selective reversible sensor for SO_3 or SO_2 detection.

Received: 23 February 2021; Accepted: 24 August 2021
Published online: 13 September 2021

References

1. Zeng, Y. *et al.* Rapid and selective H_2S detection of hierarchical $ZnSnO_3$ nanocages. *Sens. Actuator B* **159**, 245–250 (2011).
2. Bari, R. H., Patil, P. P., Patil, S. B. & Bari, A. R. Detection of H_2S gas at lower operating temperature using sprayed nanostructured In_2O_3 thin films. *Bull. Mater. Sci.* **36**, 967–972 (2013).
3. Guo, Y. Y., Li, Y., Zhu, T. Y. & Ye, M. Investigation of SO_2 and NO adsorption species on activated carbon and the mechanism of NO promotion effect on SO_2. *Fuel* **143**, 536–542 (2015).
4. Chatterjee, C. & Sen, A. Sensitive colorimetric sensors for visual detection of carbon dioxide and sulfur dioxide. *J. Mater. Chem. A* **3**, 5642–5647 (2015).
5. Robinson, E. & Robbins, R. C. Gaseous sulfur pollutants from urban and natural sources. *J. Air Pollut. Control Assoc.* **29**, 164–165 (1979).
6. Klimont, Z., Smith, S. J. & Cofala, J. The last decade of global anthropogenic sulfur dioxide: 2000–2011 emissions. *Environ. Res. Lett.* **8**, 014003 (2013).
7. Kikuchi, R. Environmental management of sulfur trioxide emission: Impact of SO_3 on human health. *Environ. Manag.* **27**, 837–844 (2001).
8. Kampa, M. & Castanas, E. Human health effects of air pollution. *Environ. Pollut.* **151**, 362–367 (2008).
9. Khan, M. A. H., Rao, M. V. & Li, Q. Recent advances in electrochemical sensors for detecting toxic gases: NO_2, SO_2 and H_2S. *Sensors* **19**, 905 (2019).
10. Selene, C. H. & Chou, J. Hydrogen sulfide: Human health aspects. *Concise International Chemical Assessment Document* **53,** (2003).
11. Khan, R. R. & Siddiqui, M. J. A. Review on effects of particulates, sulfur dioxide and nitrogen dioxide on human health. *Int. Res. J. Environ. Sci.* **3**, 70–73 (2014).
12. Solomon, D., Zhao, F. J. & Mcgrath, S. P. Atmospheric SO_2 emissions since the late 1800s change organic sulfur forms in humic substance extracts of soils. *Environ. Sci. Technol.* **42**, 3550–3555 (2008).
13. Yu, Q. *et al.* Monitoring effect of SO_2 emission abatement on recovery of acidified soil and streamwater in southwest china. *Environ. Sci. Technol.* **51**, 9498–9506 (2017).
14. Li, H. L. *et al.* Impact of SO_2 on elemental mercury oxidation over CeO_2–TiO_2 catalyst. *Chem. Eng. J.* **219**, 319–326 (2013).
15. Machida, M., Kawada, T., Yamashita, H. & Tajiri, T. Role of oxygen vacancies in catalytic SO_3 decomposition over $Cu_2V_2O_7$ in solar thermochemical water splitting cycles. *J. Phys. Chem. C* **117**, 26710–26715 (2013).
16. Smirnov, M. Y., Kalinkin, A. V., Pashis, A. V., Prosvirin, I. P. & Bukhtiyarov, V. I. Interaction of SO_2 with Pt model supported catalysts studied by XPS. *J. Phys. Chem. C* **118**, 22120–22135 (2014).
17. Ye, H. *et al.* SnSe monolayer: A promising candidate of SO_2 sensor with high adsorption quantity. *Appl. Surf. Sci.* **484**, 33–38 (2019).
18. Novoselov, K. S. *et al.* Electric field effect in atomically thin carbon films. *Science* **306**, 666–669 (2004).
19. Geim, A. K. & Novoselov, K. S. The rise of graphene. *Nat. Mater.* **6**, 183–191 (2007).
20. Esrafili, M. D. *et al.* A DFT study on SO_3 capture and activation over Si- or Al-doped graphene. *Chem. Phys. Lett.* **658**, 146–151 (2016).
21. Dean, C. R. *et al.* Boron nitride substrates for high-quality graphene electronics. *Nat. Nanotechnol.* **5**, 722–726 (2010).
22. Mak, K. F., Lee, C., Hone, J., Shan, J. & Heinz, T. F. Atomically thin MoS_2: A new direct-gap semiconductor. *Phys. Rev. Lett.* **105**, 136805 (2010).
23. Chhowalla, M. *et al.* The chemistry of two-dimensional layered transition metal dichalcogenide nanosheets. *Nat. Chem.* **5**, 263–275 (2013).
24. Xu, X. D., Yao, W., Xiao, D. & Heinz, T. F. Spin and pseudospins in layered transition metal dichalcogenides. *Nat. Phys.* **10**, 343–350 (2014).
25. Cai, Y. Q., Ke, Q. Q., Zhang, G. & Zhang, Y. W. Energetics, charge Transfer and magnetism of small molecules physisorbed on phosphorene. *J. Phys. Chem. C* **119**, 3102–3110 (2015).
26. Leenaerts, O., Partoens, B. & Peeters, F. M. Adsorption of H_2O, NH_3, CO, NO_2 and NO on graphene: A first-principles study. *Phys. Rev. B* **77**, 125416 (2018).
27. Kou, L., Frauenheim, T. & Chen, C. F. Phosphorene as a superior gas sensor: Selective adsorption and distinct I–V response. *J. Phys. Chem. Lett.* **5**, 2675–2681 (2014).
28. Abbas, A. N. *et al.* Black phosphorus gas sensors. *ACS Nano* **9**, 5618–5624 (2015).
29. Lalitha, M., Nataraj, Y. & Lakshmipathi, S. C decorated and doped phosphorene for gas adsorption. *Appl. Surf. Sci.* **377**, 311–323 (2016).
30. Kuang, A. *et al.* Acidic gases (CO_2, NO_2 and SO_2) capture and dissociation on metal decorated phosphorene. *Appl. Surf. Sci.* **410**, 505–512 (2017).
31. Lei, S. Y. *et al.* Capture and dissociation of dichloromethane on Fe, Ni, Pd and Pt decorated phosphorene. *Appl. Surf. Sci.* **495**, 143533 (2019).
32. Kaewmaraya, T., Ngamwongwan, L., Moontragoon, P., Karton, A. & Hussain, T. Drastic improvement in gas-sensing characteristics of phosphorene nanosheets under vacancy defects and elemental functionalization. *J. Phys. Chem. C* **122**, 20186–20193 (2018).
33. Kresse, G. & Furthmiiller, J. Efficiency of ab-initio total energy calculations for metals and semiconductors using a plane-wave basis set. *Comput. Mater. Sci.* **6**, 15–50 (1996).
34. Kresse, G. & Furthmuller, J. Efficient iterative schemes for ab initio total-energy calculations using a plane-wave basis set. *Phys. Rev. B* **54**, 11169–21118 (1996).
35. Perdew, J. P., Burke, K. & Ernzerhof, M. Generalized gradient approximation made simple. *Phys. Rev. Lett.* **77**, 3865–3868 (1996).
36. Grimme, S. Semiempirical GGA-type density functional constructed with a long-range dispersion correction. *J. Comput. Chem.* **27**, 1787–1799 (2006).
37. Li, Q. F., Duan, C. G., Wan, X. G. & Kuo, J. L. Theoretical prediction of anode materials in Li-ion batteries on layered black and blue phosphorus. *J. Phys. Chem. C* **119**, 8662–8670 (2015).
38. Li, X. B. *et al.* Structures, stabilities and electronic properties of defects in monolayer black phosphorus. *Sci. Rep.* **5**, 10848 (2015).

39. Hussain, T. *et al.* Defected and functionalized germanene-based nanosensors under sulfur comprising gas exposure. *ACS Sens.* **3**, 867–874 (2018).
40. Ienco, A., Manca, G., Peruzzini, M. & Mealli, C. Modelling strategies for the covalent. *Dalton Trans.* **47**, 17243–17256 (2018).
41. Ding, Y. & Wang, Y. L. Structural, electronic and magnetic properties of adatom adsorptions on black and blue phosphorene: A first-principles study. *J. Phys. Chem. C* **119**, 10610–10622 (2015).
42. Lei, S. Y. *et al.* Enhancing the ambient stability of few-layer black phosphorus by surface modification. *RSC Adv.* **8**, 14676–14683 (2018).

Acknowledgements

This work was supported by the National Natural Science Foundation of China (Nos. 11774052, 11774051, 61771137), the National Science Foundation of Jiangsu Province of China (No. BK20171355), and the Jiangsu Provincial Key Research and Development Program (BE2020006-1). Additionally, we acknowledge the Big Data Center of Southeast University, Advanced Computing East China Sub-center and Shanghai Supercomputer Center for the facility support on the calculations in this manuscript.

Author contributions

Yonghu Wang and Shuangying Lei wrote the main manuscript text. Ran Gao prepared figures 1-4,Xiaolong Sun prepared figures 5-8. Yonghu Wang, Shuangying Lei and Jie Chen revised the manuscript.All authors reviewed the manuscript.

Competing interests

The authors declare no competing interests.

Additional information

Supplementary Information The online version contains supplementary material available at https://doi.org/10.1038/s41598-021-97626-4.

Correspondence and requests for materials should be addressed to S.L. or J.C.

Reprints and permissions information is available at www.nature.com/reprints.

Publisher's note Springer Nature remains neutral with regard to jurisdictional claims in published maps and institutional affiliations.